Quantitative calculations of polarizations arising from the symmetric and antisymmetric exchange strictions in Tm-doped $GdMnO_3$*

Qin Ming-Hui(秦明辉)[a)†], Lin Lin(林 林)[b)], Li Lin(李 林)[b)], Jia Xing-Tao(贾兴涛)[c)], and Liu Jun-Ming(刘俊明)[b)‡]

[a)] *Institute for Advanced Materials and Laboratory of Quantum Engineering and Quantum Materials, South China Normal University, Guangzhou* 510006, *China*

[b)] *Laboratory of Solid State Microstructures, Nanjing University, Nanjing* 210093, *China*

[c)] *School of Physics and Chemistry, Henan Polytechnic University, Jiaozuo* 454000, *China*

(Received 12 September 2014; revised manuscript received 15 October 2014; published online 19 January 2015)

The ferroelectric polarization and phase diagram in Tm-doped $GdMnO_3$ are studied by means of Monte Carlo simulation based on the Mochizuki–Furukawa model. Our work well reproduces the low temperature polarization at various substitution levels observed experimentally. It is demonstrated that the Tm-doping can control the multiferroic behaviors through modulating the spin structures, resulting in the flop of the electric polarization. In addition, the polarization in the *ab*-plane cycloidal spin phase arises from comparable contributions of the symmetric exchange striction and antisymmetric exchange striction, leading to much bigger polarization than that in the *bc*-plane cycloidal spin phase where only the contribution of the latter striction is available. The phase diagram obtained in our simulation is helpful for clarifying the multiferroic properties in doped manganite systems and other related multiferroics.

Keywords: multiferroics, cycloidal spin order, polarization, Monte Carlo simulation

PACS: 75.80.+q, 75.30.Kz, 77.80.–e **DOI:** 10.1088/1674-1056/24/3/037509

1. Introduction

Multiferroics have attracted a great deal of attention over the past decades due to the potential applications and basic physical research interest.[1–3] Especially, the orthorhombic perovskite rare-earth manganites $R\mathrm{MnO_3}$ (R = Tb, Dy, $\mathrm{Eu_{1-x}Y_x}$, etc., with the crystal structure on the *ab*-plane shown in Fig. 1(a)) have been extensively addressed since the discovery of the strong magnetoelectric (ME) coupling in $\mathrm{TbMnO_3}$.[4–6] The ferroelectric (FE) polarization (P) in $R\mathrm{MnO_3}$ is generated by frustrated spin orders such as the cycloidal spin (CS) order and the E-type antiferromagnetic (E-AFM) order. It is believed that adjacent two spins S_i and S_{i+1} separated by vector $r_{i,i+1}$ can generate a local polarization $P^i_{\mathrm{AS}} \propto -r_{i,i+1} \times (S_i \times S_{i+1})$ through the antisymmetric exchange striction.[7–9] Thus, a macroscopic polarization P_{AS} is induced along the *a*-axis ($P_{\mathrm{AS}}//a$) in the *ab*-plane cycloidal spin (*ab*-CS) phase with the propagation vector along the *b*-axis, while it is induced along the *c*-axis ($P_{\mathrm{AS}}//c$) in the *bc*-plane cycloidal spin (*bc*-CS) phase. On the other hand, the very large P_{S} along the *a*-axis induced in the E-AFM order can be explained by the symmetric exchange striction associated with the inner product of the spins ($S \cdot S$).[10] In addition, some other works on these issues are reported.[11–14]

Interestingly, the low-temperature (T) multiferroic phase in $R\mathrm{MnO_3}$ is mainly determined by the magnitude of the $\mathrm{GdFeO_3}$-type distortion which depends on the size of the R ion.[15] With decreasing R-site ionic radius, four magnetic phases successively emerge at low T: the non-FE A-type antiferromagnetic (A-AFM) order, the FE *ab*-CS phase, the FE *bc*-CS phase, and the FE E-type AFM order.[16] Thus, the substitution at the R-site with proper species becomes an efficient way to modulate the multiferroic properties in $R\mathrm{MnO_3}$. Beyond $\mathrm{TbMnO_3}$ and $\mathrm{DyMnO_3}$, more multiferroic manganites of the CS order can be synthesized by this method such as $\mathrm{Eu_{1-x}Y_xMnO_3}$ and $\mathrm{Gd_{1-x}Tb_xMnO_3}$.[6,17] Recently, a microscopic spin model (M–F model) which includes the superexchange interaction, the single-ion anisotropy (SIA), the Dzyaloshinskii–Moriya (DM) interaction, and the spin–phonon coupling, was proposed and well reproduced mea-

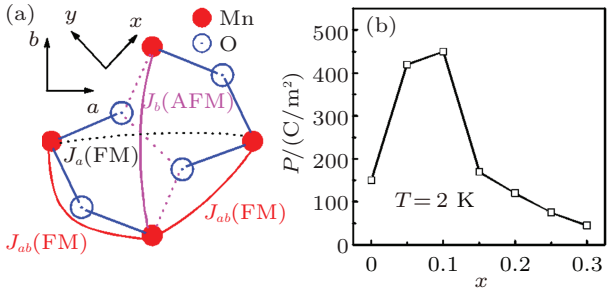


Fig. 1. (color online) (a) Crystal structure and spin-exchange interactions in orthorhombically distorted $R\mathrm{MnO_3}$ (*ab*-plane). (b) The experimentally obtained P–x data of polycrystalline $\mathrm{Gd_{1-x}Tm_xMnO_3}$ at $T = 2$ K. The polarization data are multiplied by 15 to give a reasonable estimation of P for single crystalline specimens.

*Project supported by the National Natural Science Foundation of China (Grant Nos. 11204091, 11274094, and 51332007) and the National Basic Research Program of China (Grant Nos. 2015CB921202 and 2011CB922101).

†Corresponding author. E-mail: qinmh@scnu.edu.cn

‡Corresponding author. E-mail: liujm@nju.edu.cn

© 2015 Chinese Physical Society and IOP Publishing Ltd

sured polarization and phase diagrams of RMnO$_3$.[18,19] In particular, for the *ab*-CS phase, it was predicted that both the symmetric $(S\cdot S)$-type exchange striction and antisymmetric $(S\times S)$-type exchange striction contribute to the polarization along the *a*-axis, leading to a much larger total polarization $P = P_{\rm AS} + P_{\rm S}$ in the *ab*-CS phase than that in the *bc*-CS phase, where P along the *c*-axis is purely resulted from the antisymmetric striction, i.e., $P = P_{\rm AS}$.[16] Several other experimental phenomena have been qualitatively explained based on the same or similar models.[20–24]

On the other hand, a quantitative calculation of the polarizations arising from the symmetric striction and antisymmetric striction respectively is essential to the complete understanding of the multiferroic properties in RMnO$_3$. Nevertheless, in spite of the success of the M–F model in explaining observed experiments in terms of magnetic structures and ferroelectricity, a quantitatively consistent calculation of the FE polarization has been less available.[23] In addition, related experimental data have been rare either although Sm$_{1-x}$Y$_x$MnO$_3$ was investigated in terms of P as a function of x,[25] since a reliable evaluation of $P_{\rm AS}$ and $P_{\rm S}$ from the measured total polarization P is a tough issue, making a quantitative and even qualitative comparison between experiments and the M–F model calculation challenging. In a recent experiment, we reported the evaluated data on $P_{\rm AS}$ and $P_{\rm S}$ associated with the *ab*-CS phase in Gd$_{1-x}$Tb$_x$MnO$_3$ where the GdMnO$_3$ is located at the boundary between the A-AFM phase and *ab*-CS phase, and a slight substitution of Gd^{3+} by much smaller Tm^{3+} allows a gradual evolution of the magnetic phase from the A-AFM phase into the *ab*-CS phase before eventually evolving into the *bc*-CS phase where no component $P_{\rm S}$ is available.[26] This allows us a specific platform at which the M–F model can be employed to calculate the $P_{\rm AS}$ and $P_{\rm S}$ in the quantitative sense. This study may provide clues to enlarge polarization and enhance the ME coupling in similar multiferroics, which is thus of particular significance.

Figure 1(b) shows the measured P at $T = 2$ K as a function of x in Gd$_{1-x}$Tb$_x$MnO$_3$, noting here that we multiply the polarization data by 15 since our samples are polycrystalline. It was repeatedly confirmed that the P measured from single crystal samples is roughly 10–15 times that from the polycrystalline samples, while a quantitative consistency between experiment and theory on the same order of magnitude is already satisfactory. In this work, we start from the M–F model with the Mn spin $S = 2$ on a cuboidal lattice and perform quantitative calculations on the polarizations of Gd$_{1-x}$Tb$_x$MnO$_3$ and then compare them with measured results. The experimental results can be well reproduced, and the phase diagram at low T obtained by means of Monte Carlo simulation is discussed in detail.

The remainder of this paper is organized as follows: In Section 2 the model and the simulation method will be described. Section 3 is attributed to the simulation results and discussion. Finally, the conclusion is presented in Section 4.

2. Model and method

The Hamiltonian can be written as $H = H_{\rm ex} + H_{\rm sia} + H_{\rm DM} + H_K$. The first term $H_{\rm ex} = \sum_{\langle i,j\rangle} J_{ij}(S_i \cdot S_j)$ denotes the spin exchange interactions, where $J_a = -0.1$ and J_b are the coupling constants in the Mn–Mn bonds on the *ab* plane, the Peierls-type spin–phonon coupling $J_{ij} = J_{ab} + J'_{ab}\delta_{i,j}$ with $J_{ab} = -0.8$ and $J'_{ab} = 2.5$ is considered for the Mn–O–Mn bonds along the x axis and the y axis (Fig. 1(a)),[23] $\delta_{i,j}$ denotes a further shift of the O ion between the i-th and j-th Mn ions normalized by the Mn–O bond length, and $J_c = 1.2$ is the strong AFM exchange in the Mn–Mn bonds along the *c*-axis. Here the energy unit is meV. The second term is the single-ion anisotropy, which consists of two parts as $H_{\rm sia} = D\sum_i S^i_{\xi i} + E\sum_i (-1)^{i_x+i_y}(S^i_{\xi i} - S^i_{\eta i})$ with $D = 0.2$ and $E = 0.3$. Here, ξ_i, η_i, ζ_i are the tilted local axes attached to the i-th MnO$_6$ octahedron, i_x, i_y, and i_z represent the integer coordinates of the i-th Mn ion. For their direction vectors, we use the experimental data of GdMnO$_3$.[27] The third term $H_{\rm DM}$ represents the DM interactions which can be expressed by $H_{\rm DM} = \sum_{\langle i,j\rangle} d_{i,j}(S_i \times S_j)$. Here the DM vectors $d_{i,j}$ are determined by five DM parameters, $(\alpha_{ab}, \beta_{ab}, \gamma_{ab}) = (0.10, 0.10, 0.14)$ and $(\alpha_c, \beta_c) = (0.45, 0.1)$. The fourth term $H_K = K\sum_i(\delta^2_{i,i+x} + \delta^2_{i,i+y})$ represents the lattice elastic term, $K = 400$ is the elastic constant.

The values of J_a, J_{ab}, J_c, J'_{ab}, D, E, K, and five DM parameters for several RMnO$_3$ systems have been microscopically determined or estimated in earlier work.[19] In addition, it is noted that the exchange path for J_b contains two O 2p orbitals, whose hybridization can be enhanced by the orthorhombic distortion. Thus, J_b can be treated as a variable which increases as the R-site ionic radius decreases. Our simulation is performed on a $36\times 36\times 6$ cuboidal lattice with periodic boundary conditions using the standard Metropolis algorithm and temperature exchange method.[28,29] The specific heat $C(T) = (\langle H^2\rangle - \langle H\rangle^2)/Nk_{\rm B}T^2$ and spin-helicity vector $h_\gamma(T) = \langle|\sum_i S_i \times S_{i+b}|\rangle/NS^2$ $(\gamma = a,b,c)$ are calculated to determine the transition points and the spin structures, here N is the number of Mn ions, $k_{\rm B}$ is the Boltzmann constant, and the brackets denote thermal and configuration averaging. It is expected that h_c (h_a) has a large value in the *ab*-CS (*bc*-CS) order, while the other two components of h are strongly suppressed. On the other hand, all these three components of h should be nearly equal to zero in the paramagnetic (PM), A-AFM and sinusoidal collinear antiferromagnetic (sc-AFM) phases. In addition, based on the point charge model, the electric polarization $P_{\rm S} = (P^a_{\rm S}, P^b_{\rm S}, P^c_{\rm S})$ due to the oxygen displacements $\delta_{i,j}$ induced by the symmetric exchange

striction can be expressed by $P_\gamma = -\prod\sum_i[(-1)^{i_x+i_y+m}\delta_{i,i+x} + (-1)^{i_x+i_y+n}\delta_{i,i+y}]/N$, where $(m,n) = (0,0)$ for $\gamma = a$, $(m,n) = (1,0)$ for $\gamma = b$, and $(m,n) = (i_z+1, i_z+1)$ for $\gamma = c$. The constant $\prod$ is estimated to be 2×10^5 μC/m^2, which is comparable with the earlier calculation.

3. Simulation results and discussion

The simulated specific heat $C(T)$, spin helicity $h_\gamma(T)$, and polarization $P_S(T)$ due to the symmetric $(S\cdot S)$-type exchange striction for a small value of $J_b = 0.5$ meV are presented in Fig. 2. A single phase transition can be observed in the $C(T)$ curve, which corresponds to the transition from the PM phase into the A-AFM phase. The spin helicity vector h is nearly equal to zero constantly through this transition, and the electric polarization P_S in the A-AFM phase is extrapolated to zero at $T\to0$ (Fig. 2(b)). In fact, it was experimentally noted that $GdMnO_3$ is of the A-AFM state at low T but close to the boundary between the A-AFM order and the CS order.[30,31] Hence, the electric polarization at $x = 0$ observed in an earlier experiment may be due to the inhomogeneity caused by the inevitable chemical disorder and defects in realistic materials.[32]

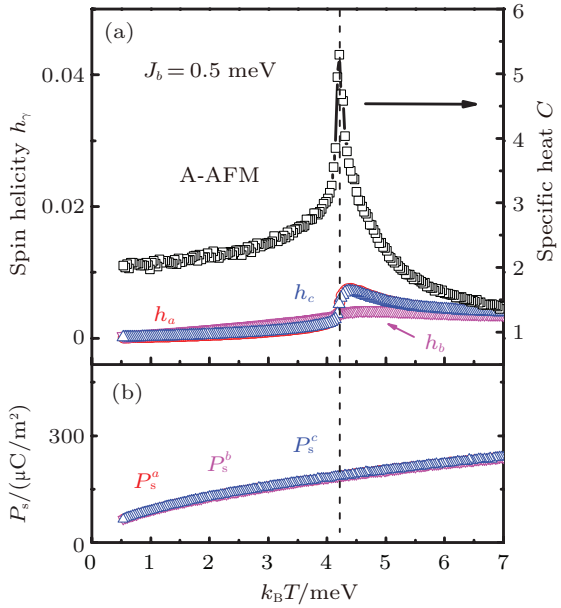


Fig. 2. (color online) (a) Specific heat $C(T)$, spin-helicity vector $h_\gamma(T)$ $(\gamma = a,b,c)$, and (b) polarizations due to the symmetric $(S\cdot S)$-type exchange striction $P_S(T)$ as a function of T for $J_b = 0.5$ meV.

The J_b is increased with increasing x. In Figs. 3(a) and 3(b), we show the calculated results for a larger value of $J_b = 0.8$ meV. Three successive phase transitions occur with decreasing T. The first one is the transition from the PM state to the sc-AFM state. The second one is the transition into the *bc*-CS order in which P_{AS} is induced along the *c*-axis. When T further falls down to the third transition point, h_c steeply increases, accompanied

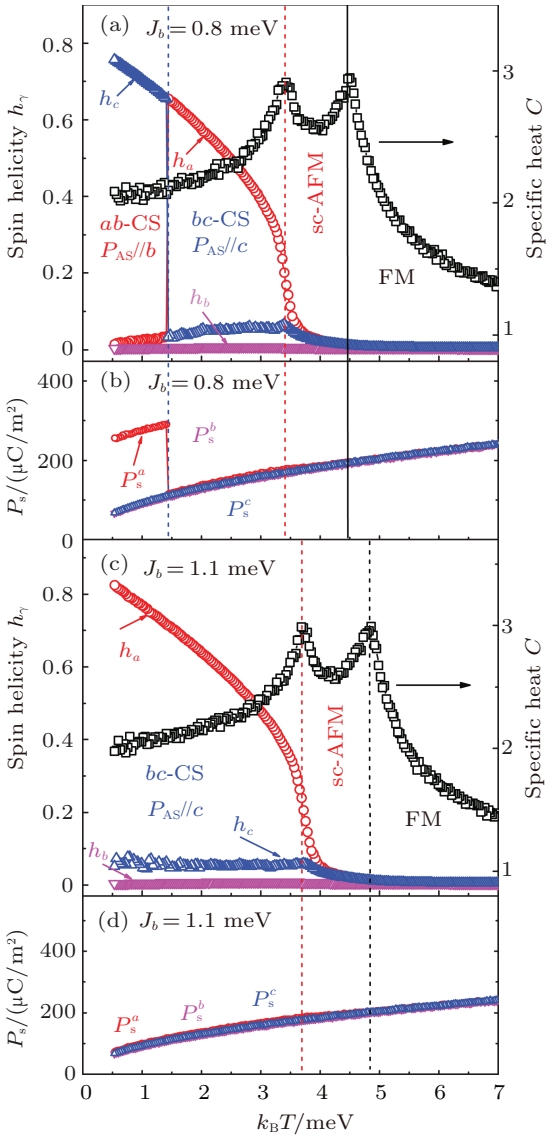


Fig. 3. (color online) $C(T)$, $h_\gamma(T)$ $(\gamma = a,b,c)$ as a function of T for (a) $J_b = 0.8$ meV and (c) $J_b = 1.1$ meV, and $P_S(T)$ as a function of T for (b) $J_b = 0.8$ meV and (d) $J_b = 1.1$ meV.

with the sudden drop of h_a, clearly indicating the occurrence of the transition from the *bc*-CS order to the *ab*-CS order. In addition, P_S^a equals to ~ 250 μC/m^2 at low T in the *ab*-CS phase (Fig. 3(b)), indicating a finite contribution of the symmetric $(S\cdot S)$-type exchange striction to the ferroelectric polarization. The $(S\cdot S)$ contribution may be understood from the energy landscape. The *ab*-CS order is stabilized by the SIA and the DM interaction with vectors on the in-plane Mn–O–Mn bonds. In the absence of the DM interaction and the spin–phonon coupling, the spins rotate with the same rotation angles of ϕ_{ab} satisfying relation $\cos\phi_{ab} = J_{ab}/(2J_b)$. When the DM interaction is introduced, these angles are alternately modulated into $\phi_{ab}+\Delta\phi_{ab}$ and $\phi_{ab}-\Delta\phi_{ab}$ with $\Delta\phi_{ab} > 0$ in order to get an energy gain. At the same time, the O ions between two spins with a smaller angle of $\phi_{ab}-\Delta\phi_{ab}$ (a larger angle of $\phi_{ab}+\Delta\phi_{ab}$) shift negatively (positively) to strengthen (weaken) the ferromagnetic exchange due to the spin–phonon coupling, leading

to the generation of the macroscopic ferroelectric polarization. On the other hand, the induced polarizations between neighboring *ab* planes can be perfectly cancelled in the *bc*-CS order. As a result, there is no contribution to the ferroelectric polarization from the $(S\cdot S)$-type exchange striction in the *bc*-CS order.

The third transition point shifts toward the low-T side and eventually disappears as J_b further increases, indicating the flops of the spiral-plane from the *ab*-plane to the *bc* plane. $C(T)$ shows two peaks and h_c is small over the whole T-range for $J_b = 1.1$ meV (Fig. 3(c)), indicating that the *ab*-CS order is completely suppressed and the *bc*-CS order occupies the whole T-range below the second transition point. Similarly, three components of P_S in the *bc*-CS phase are respectively extrapolated to zero at $T \to 0$, as clearly shown in Fig. 3(d). The ferroelectric polarization along the *c*-axis uniquely originated from the contribution of the antisymmetric $(S\times S)$-type exchange striction, as reported earlier.

In order to have a quantitative comparison between our calculated polarization and the experimental results, we also calculate the $(S\times S)$ contribution at $T \to 0$. Based on the spin-current theory, P_{AS} is proportional to the spin helicity h. In this work, the proportionality factor is estimated to be 200 μC/m^2 due to the fact that the observed P_{AS} in the *bc*-CS order is ~200 μC/m^2 for Tb-doped $GdMnO_3$.[17] In Fig. 4, the calculated J_b dependence of P_S, P_{AS}, and $P_S + P_{AS}$ at $T \to 0$ are respectively presented. The simulated $P_S + P_{AS}$ reproduces well the experimental polarization which is also given for a clear comparison. As a result, our quantitative calculation shows good consistency with experiment results, and one may give a firm interpretation about the multiferroicity in $Gd_{1-x}Tb_xMnO_3$. For small x, the *ab*-CS order is stabilized at low T, and remarkable polarization arises from the contributions of both the symmetric $(S\cdot S)$-type exchange striction and the antisymmetric $(S\times S)$-type exchange striction can be observed. With further Tm-substitution, the *ab*-CS order is replaced by the *bc*-CS order in which only the antisymmetric exchange striction contributes to the polarization, leading to the significant reduction of the polarization.

It is noted that the measured polarization is gradually reduced with further substitution in the experiment. This phenomenon is not reproduced in our simulation in which the polarization remains almost the same in the whole region with the *bc*-CS order. In fact, a similar result has been reported in an earlier simulation.[19] The inconsistency between the theory and experiment may be due to the fact that the inevitable inhomogeneity in realistic materials is completely ignored in simulations. However, our work uncovers the multiferroic phases in $Gd_{1-x}Tb_xMnO_3$, and confirms the important role of the spin–phonon coupling in the modulation of polarization in similar multiferroic materials.

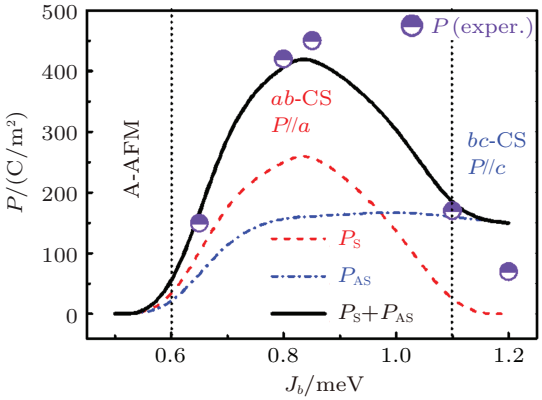


Fig. 4. (color online) Calculated J_b dependence of $(S\cdot S)$ contribution P_S, $(S\times S)$ contribution P_{AS}, and the summation $P_S + P_{AS}$ at $T \to 0$. The summation reproduces the experimental P well.

4. Conclusion

In conclusion, we have systematically investigated the multiferroic properties in the Tm-substituted $GdMnO_3$ with Monte Carlo simulation of the M–F model. The experimental polarization can be well reproduced, and the phase diagram at low temperature is microscopically determined. The relatively large polarization at the low substitution level is proved to be caused by the contributions of both the symmetric $(S\cdot S)$-type exchange striction and the antisymmetric $(S\times S)$-type exchange striction in the *ab*-CS phase. With further substitution, a phase transition from the *ab*-CS order to the *bc*-CS order occurs, and the polarization is significantly reduced due to the fact that only the $(S\times S)$-type exchange striction contributes to the polarization in the *bc*-CS order. This work is helpful for clarifying the multiferroic behaviors observed in doped manganite systems and other related multiferroic materials.

References

[1] Cheong S W and Mostovoy M 2007 *Nat. Mater.* **6** 13
[2] Wang K F, Liu J M and Ren Z F 2009 *Adv. Phys.* **58** 321
[3] Lunkenheimer P, Muller J, Krohns S, Schrettle F, Loidl A, Hartmann B, Rommel R, Desouza M, Hotta C, Schlueter J A and Lang M 2012 *Nat. Mater.* **11** 755
[4] Kimura T, Goto T, Shintani T H, Ishizaka K, Arima T and Tokura Y 2003 *Nature* **426** 55
[5] Goto T, Kimura T, Lawes G, Ramirez A P and Tokura Y 2004 *Phys. Rev. Lett.* **92** 257201
[6] Hemberger J, Schrettle F, Pimenov A, Lunkenheimer P, Ivanov V Y, Mukhin A A, Balbashov A M and Loidl A 2007 *Phys. Rev. B* **75** 035118
[7] Katsura H, Nagaosa N and Balatsky A V 2005 *Phys. Rev. Lett.* **95** 057205
[8] Mostovoy M 2006 *Phys. Rev. Lett.* **96** 067601
[9] Sergienko I A and Dagotto E 2006 *Phys. Rev. B* **73** 094434
[10] Arima T, Tokunaga A, Goto T, Kimura H, Noda Y and Tokura Y 2006 *Phys. Rev. Lett.* **96** 097202
[11] Jia C L, Onoda S, Nagaosa N and Han J H 2007 *Phys. Rev. B* **76** 144424
[12] Xiang H J, Kan E J, Zhang Y, Whangbo M H and Gong X G 2011 *Phys. Rev. Lett.* **107** 157202
[13] Chen H B, Zhou Y and Li Y Q 2013 *J. Phys.: Condens. Matter* **25** 286004
[14] Tanabe Y, Moriya T and Sugano S 1965 *Phys. Rev. Lett.* **15** 1023
[15] Zhou T, Wang H T, Hong B, Tao Q and Xu Z A 2011 *Chin. Phys. Lett.* **28** 027501
[16] Ishiwata S, Kaneko Y, Tokunaga Y, Taguchi Y, Arima T H and Tokura Y 2010 *Phys. Rev. B* **81** 100411

[17] Goto T, Yamasaki Y, Watanabe H, Kimura T and Tokura Y 2005 *Phys. Rev. B* **72** 220403
[18] Mochizuki M and Furukawa N 2009 *Phys. Rev. B* **80** 134416
[19] Mochizuki M, Furukawa N and Nagaosa N 2011 *Phys. Rev. B* **84** 144409
[20] Mochizuki M and Furukawa N 2010 *Phys. Rev. Lett.* **105** 187601
[21] Mochizuki M, Furukawa N and Nagaosa N 2010 *Phys. Rev. Lett.* **104** 177206
[22] Mochizuki M and Nagaosa N 2010 *Phys. Rev. Lett.* **105** 147202
[23] Mochizuki M, Furukawa N and Nagaosa N 2010 *Phys. Rev. Lett.* **105** 037205
[24] Qin M H, Tao Y M, Dong S, Zhao H B, Gao X S and Liu J M 2011 *Appl. Phys. Lett.* **98** 102510
[25] Flynn D O, Tomy C V, Lees M R, Aladine A D and Balakrishnan G 2011 *Phys. Rev. B* **83** 174426
[26] Li L, Lin L, Yan Z B, He Q Y and Liu J M 2012 *J. Appl. Phys.* **112** 034115
[27] Mori T, Kamegashira N, Aoki K, Shishido T and Fukuda T 2002 *Mater. Lett.* **54** 238
[28] Landau D P and Binder K 2005 *A Guide to Monte Carlo Simulations in Statistical Physics* (Cambridge: Cambridge University Press)
[29] Hukushima K and Nemoto K 1996 *J. Phys. Soc. Jpn.* **65** 1604
[30] Kimura T, Lawes G, Goto T, Tokura Y and Ramirez A P 2005 *Phys. Rev. B* **71** 224425
[31] Dong S and Liu J M 2012 *Mod. Phys. Lett.* **26** 1230004
[32] Liu J M, Chan L W and Choy C L 2009 *Chin. Phys. Lett.* **26** 087501